Supplementary Information (SI) for Faraday Discussions.

Supporting Information

Designing Anti-bacterial Supramolecular Gels from Primary Ammonium Dicarboxylate (PAD) salts for Self-Delivery Applications.

Authors Nabanita Roy, Subhajit Ghosh, Abhishek Dutta and Parthasarathi Dastidar*

Affiliation School of Chemical Sciences, Indian Association for the Cultivation of Science (IACS), 2A and 2B, Raja S. C. Mullick Road, Jadavpur, Kolkata-700032, West Bengal (India).

E mail. ocpdastidar@gmail.com, ocpd@iacs.res.in

Table of Contents

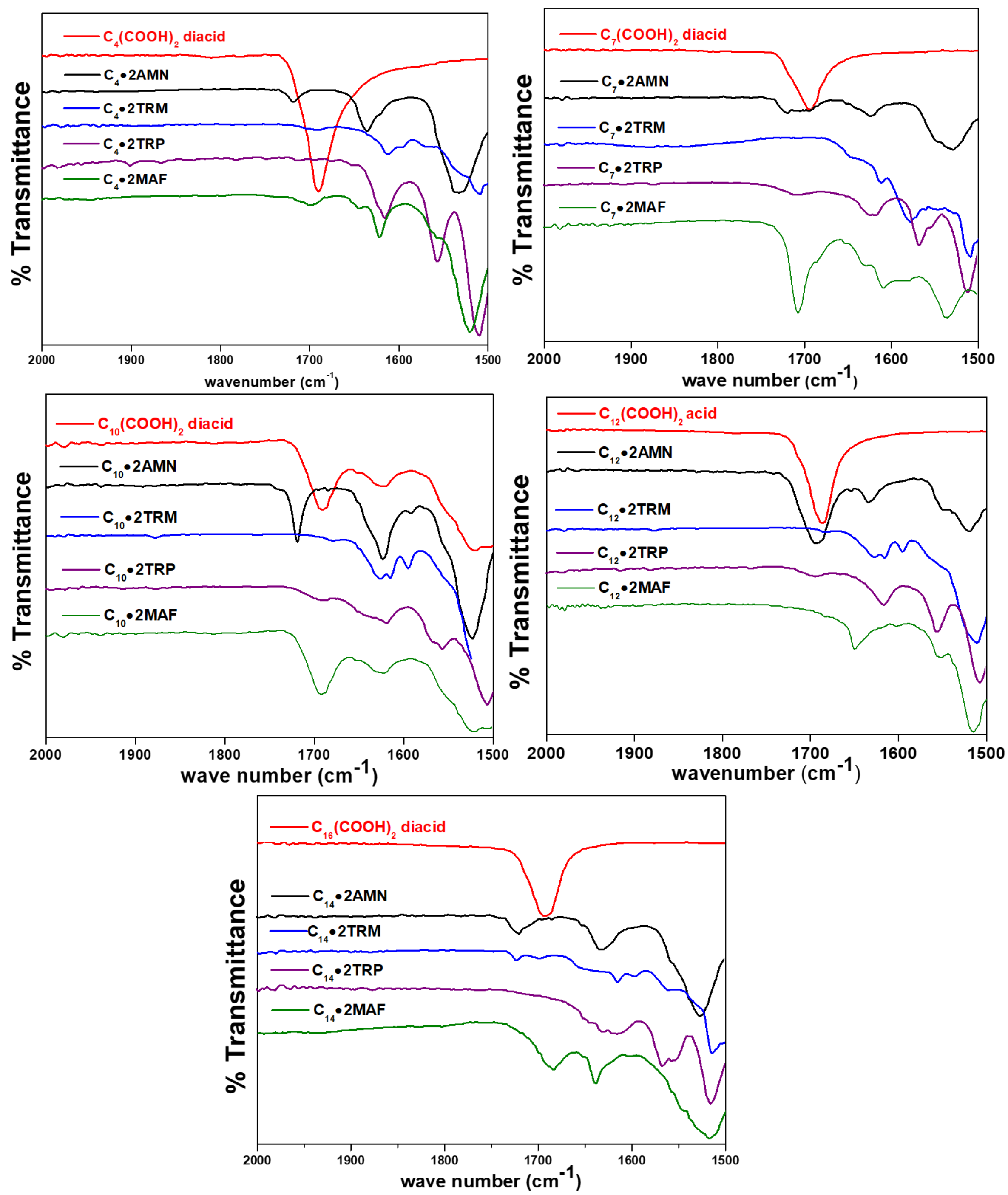

Fig. S1 FT-IR spectra of the salts.

Table S1 Approximate shifts in the FT-IR stretching frequencies upon salt formation from carboxylic acids to carboxylates.

Dicarboxylic acids	IR str. Freq. of >COOH in diacids	Salts	IR str. Freq. of >COO$^-$ in salts	$\Delta\bar{\nu}$ shifts in salts
$C_4(COOH)_2$	1690	C_4•2AMN	1636	54
		C_4•2TRM	1613	77
		C_4•2TRP	1616	74
		C_4•2MAF	1622	68
$C_7(COOH)_2$	1693	C_7•2AMN	1625	68
		C_7•2TRM	1612	81
		C_7•2TRP	1622	71
		C_7•2MAF	1707, 1631	-14
$C_{10}(COOH)_2$	1691	C_{10}•2AMN	1719, 1623	-28
		C_{10}•2TRM	1629	62
		C_{10}•2TRP	1644	47
		C_{10}•2MAF	1691, 1624	0
$C_{12}(COOH)_2$	1690	C_{12}•2AMN	1693, 1635	-3
		C_{12}•2TRM	1629	61
		C_{12}•2TRP	1617	73
		C_{12}•2MAF	1651	39
$C_{14}(COOH)_2$	1692	C_{14}•2AMN	1720, 1632	-28
		C_{14}•2TRM	1616	76
		C_{14}•2TRP	1617	75
		C_{14}•2MAF	1681	11

Table S2 Gelation table

Organic salts	water	Methyl salicylate (MS)	19 DMSO/water	11 DMSO/water
C_4•2AMN	P	GP	P	P
C_4•2TRM	S	GP	S	S
C_4•2TRP	S	P	S	S
C_4•2MAF	S	INS	S	S
C_7•2AMN	P	**G**	P	P
C_7•2TRM	S	PS	S	S
C_7•2TRP	S	GP	S	S
C_7•2MAF	S	GP	P	S
C_{10}•2AMN	P	**G**	P	P
C_{10}•2TRM	S	P	S	S
C_{10}•2TRP	INS	P	P	S
C_{10}•2MAF	S	P	WG	S
C_{12}•2AMN	INS	**G**	INS	P

C_{12}•2TRM	PS	**G**	INS	S
C_{12}•2TRP	PS	**G**	INS	S
C_{12}•2MAF	GP	**G**	P	S
C_{14}•2AMN	INS	**G**	P	P
C_{14}•2TRM	P	GP	INS	S
C_{14}•2TRP	P	GP	INS	S
C_{14}•2MAF	GP	**G**	P	S

S= Soluble; **PS**= Partially soluble; **INS**=Insoluble; **P**=Precipitate; **GP**=Gelatinous precipitate; **G**=Gel

Table S3 MGC and T_{gel} table for various gels.

Gels	Solvent	MGC	T_{gel} at 10 wt. % (in °C)
C_7●2AMN	MS	8	65
C_{10}●2AMN	MS	8	57
C_{12}●2AMN	MS	10	52
C_{12}●2TRM	MS	10	87
C_{12}●2TRP	MS	6	85
C_{12}●2MAF	MS	10	72
C_{14}●2AMN	MS	10	64
C_{14}●2MAF	MS	8	89

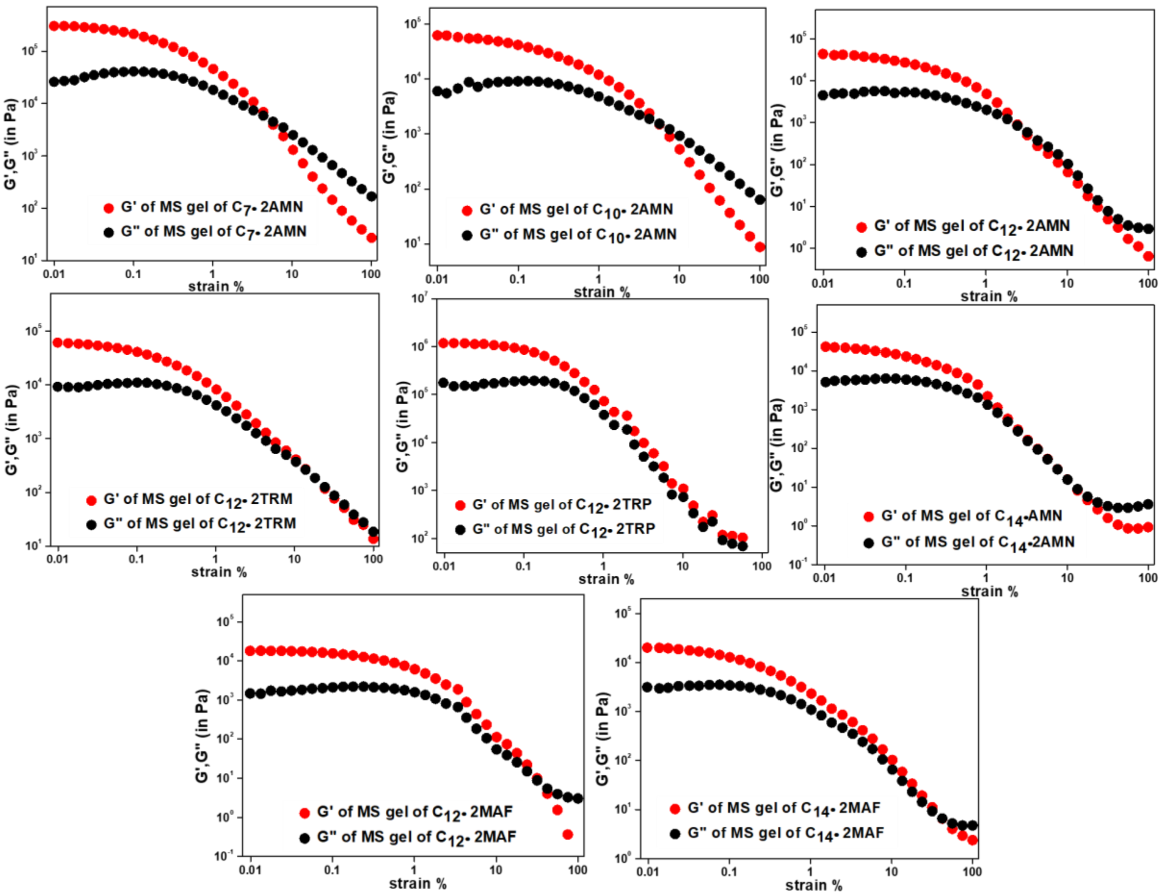

Fig. S2 Amplitude sweep experiments of the 10 wt. % MS gels

Table S4 tan δ (G"/G') values of the reported gels.

Gels	G'(in Pa)	G" (in Pa)	tan δ (G"/G')
C_7•2AMN	362687.5	49156.25	**0.135**
C_{10}•2AMN	114337.5	17633.75	**0.162**
C_{12}•2AMN	90568.75	12698.125	**0.144**
C_{12}•2TRM	207625	45412.5	**0.235**
C_{12}•2TRP	557937.5	85593.75	**0.156**
C_{12}•2MAF	15875	4491.875	**0.284**
C_{14}•2AMN	23956.25	2879.375	**0.124**
C_{14}•2MAF	32200	7250.625	**0.241**

Table S5 Crystallographic data table.

	C_4•2AMN	C_4•2TRM	C_4•2TRP	C_4•2MAF	C_7•2AMN	C_{10}-H•AMN	C_{10}•2TRM	C_{10}•2TRP	[C_{14}•2MAF].C_{14}-H_2
Crystallising solvent	MeOH	EtOH	MeOH+ DCM	H2O+ MeOH	MeOH	MeOH	DMSO	MeOH+ DCM	MeOH+ DCM
Empirical formula	$C_{26}H_{44}N_2O_4$	$C_{33}H_{48}N_3O_9$	$C_{26}H_{34}N_4O_4$	$C_{20}H_{22}N_4O_8S_2$	$C_{29}H_{50}N_2O_4$	$C_{22}H_{39}NO_4$	$C_{28}H_{44}N_2O_6$	$C_{32}H_{46}N_4O_4$	$C_{23}H_{40}N_2O_6S$
Formula weight	448.63	630.74	466.57	510.53	490.71	381.54	504.65	550.73	472.63
Temperature/K	146.55	145.01	296.15	147.9	273.15	273.15	298.66	296.15	295.75
Crystal system	triclinic	triclinic	monoclinic	monoclinic	monoclinic	triclinic	orthorhombic	triclinic	triclinic
Space group	$P\bar{1}$	$P\bar{1}$	$P2_1/n$	$P2_1/n$	$P2_1/c$	$P\bar{1}$	$Pca2_1$	$P\bar{1}$	$P\bar{1}$
a/Å	6.5625(4)	11.4038(8)	9.788(6)	10.4623(3)	20.775(19)	6.683(2)	21.69(3)	6.4847(19)	5.8262(16)
b/Å	13.4728(9)	12.7819(7)	6.098(4)	5.9160(2)	6.448(6)	13.220(4)	6.077(8)	7.741(2)	9.250(3)
c/Å	14.2734(8)	13.6007(8)	21.090(14)	20.1437(6)	21.727(19)	13.306(4)	22.48(3)	16.693(5)	24.521(7)
α/°	75.183(2)	88.897(2)	90	90	90	107.090(4)	90	91.501(4)	79.998(8)
β/°	78.290(2)	70.005(2)	96.993(9)	104.9680(10)	97.79(3)	91.044(5)	90	98.704(4)	88.376(9)
γ/°	80.854(2)	65.733(2)	90	90	90	96.239(4)	90	108.733(4)	80.227(9)
Volume/$Å^3$	1186.97(13)	1681.25(18)	1249.3(14)	1204.49(6)	2884(4)	1115.5(6)	2963(7)	781.9(4)	1282.5(6)
Z	2	2	2	2	4	2	4	1	2
$\rho_{calc}g/cm^3$	1.255	1.246	1.240	1.408	1.130	1.136	1.131	1.170	1.224
μ/mm^{-1}	0.054	0.090	0.085	0.273	0.074	0.077	0.079	0.077	0.165
F(000)	492.0	678.0	500.0	532.0	1080.0	420.0	1096.0	298.0	512.0
Crystal size/mm^3	0.2 × 0.05 × 0.04	0.4 × 0.03 × 0.02	0.4 × 0.1 × 0.03	0.3 × 0.04 × 0.02	0.4 × 0.03 × 0.02	0.3 × 0.03 × 0.02	0.1 × 0.03 × 0.02	0.4 × 0.04 × 0.03	0.2 × 0.05 × 0.03
Radiation	AgKα (λ = 0.56086)	MoKα (λ = 0.71073)	MoKα (λ = 0.71073)	MoKα (λ = 0.71073)	MoKα (λ = 0.71073)	MoKα (λ = 0.71073)	MoKα (λ = 0.71073)	MoKα (λ = 0.71073)	MoKα (λ = 0.71073)
2Θ range for data collection/°	3.804 to 50.82	4.588 to 50.938	3.892 to 50.05	6.528 to 63.408	1.978 to 53.266	3.206 to 50.218	5.22 to 50.47	4.954 to 51.148	4.536 to 56.542
Index ranges	-10 ≤ h ≤ 9, -19 ≤ k ≤ 20, -21 ≤ l ≤ 17	-13 ≤ h ≤ 13, -15 ≤ k ≤ 15, -16 ≤ l ≤ 15	-11 ≤ h ≤ 11, -7 ≤ k ≤ 7, -25 ≤ l ≤ 25	-15 ≤ h ≤ 14, -8 ≤ k ≤ 7, -29 ≤ l ≤ 29	-25 ≤ h ≤ 26, -7 ≤ k ≤ 7, -25 ≤ l ≤ 25	-7 ≤ h ≤ 7, -15 ≤ k ≤ 15, -15 ≤ l ≤ 15	-26 ≤ h ≤ 26, -7 ≤ k ≤ 7, -26 ≤ l ≤ 26	-7 ≤ h ≤ 7, -9 ≤ k ≤ 9, -20 ≤ l ≤ 20	-7 ≤ h ≤ 7, -12 ≤ k ≤ 12, -32 ≤ l ≤ 28
Reflections collected	15179	16204	17992	16545	42337	16637	24367	12445	14756
Independent reflections	7620 [R_{int} = 0.0586, R_{sigma} = 0.0824]	6172 [R_{int} = 0.0501, R_{sigma} = 0.0641]	2211 [R_{int} = 0.0323, R_{sigma} = 0.0182]	3967 [R_{int} = 0.0548, R_{sigma} = 0.0495]	5274 [R_{int} = 0.1004, R_{sigma} = 0.0600]	3952 [R_{int} = 0.0680, R_{sigma} = 0.0666]	5191 [R_{int} = 0.0719, R_{sigma} = 0.0659]	2934 [R_{int} = 0.0560, R_{sigma} = 0.0561]	6313 [R_{int} = 0.0624, R_{sigma} = 0.0831]
Data/restraints/parameters	7620/0/465	6172/0/413	2211/0/156	3967/0/164	5274/0/319	3952/51/254	5191/71/341	2934/0/182	6313/2/333
Goodness-of-fit on F^2	1.028	1.012	1.063	1.036	1.024	1.034	1.046	1.000	1.108
Final R indexes [I>=2σ (I)]	R_1 = 0.0578, wR_2 = 0.1435	R_1 = 0.0438, wR_2 = 0.0930	R_1 = 0.0362, wR_2 = 0.0909	R_1 = 0.0540, wR_2 = 0.1553	R_1 = 0.0617, wR_2 = 0.1543	R_1 = 0.0496, wR_2 = 0.1294	R_1 = 0.0682, wR_2 = 0.1531	R_1 = 0.0506, wR_2 = 0.1078	R_1 = 0.1055, wR_2 = 0.2621
Final R indexes [all data]	R_1 = 0.0799, wR_2 = 0.1675	R_1 = 0.0746, wR_2 = 0.1086	R_1 = 0.0439, wR_2 = 0.0964	R_1 = 0.0650, wR_2 = 0.1671	R_1 = 0.1216, wR_2 = 0.1885	R_1 = 0.0846, wR_2 = 0.1502	R_1 = 0.1345, wR_2 = 0.1884	R_1 = 0.1053, wR_2 = 0.1312	R_1 = 0.1417, wR_2 = 0.2829
Largest diff. peak/hole / e $Å^{-3}$	0.45/-0.36	0.21/-0.21	0.19/-0.17	0.86/-0.83	0.35/-0.26	0.20/-0.20	0.44/-0.50	0.16/-0.16	0.59/-0.47

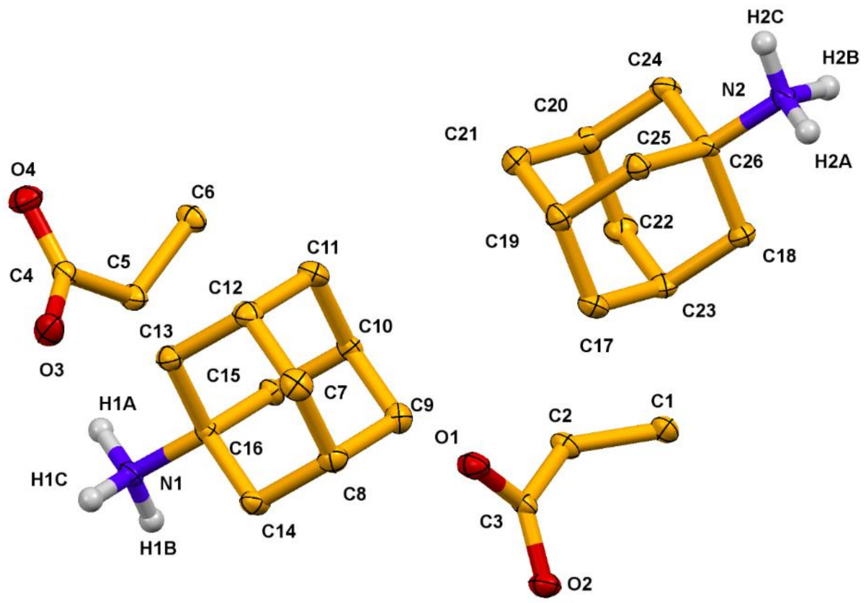

Fig. S3 ORTEP diagram of C_4•2AMN (50% probability).

Table S6 Hydrogen bonding table of C_4•2AMN.

D-H•••A	d(D-A)/Å	d(H•••A)/Å	d(D•••A)/Å	∠D-H•••A/°	Symmetry
N1-H1A•••O3	0.98	1.85	2.8176(16)	167	x,y,z
N2-H1B•••O4	0.93	1.79	2.7165(16)	172	-x+1,y,-z
N1-H1C•••O1	0.93	1.87	2.7838(15)	169	-x,1-y,2-z
N2-H2A•••O2	1.00	1.80	2.7795(16)	166	-x,-1+y,z
N2-H2B•••O3	0.93	1.89	2.8035(16)	168	1-x,-y,2-z
N1-H2C•••O1	0.93	1.89	2.7994(16)	135	-x,-y,2-z

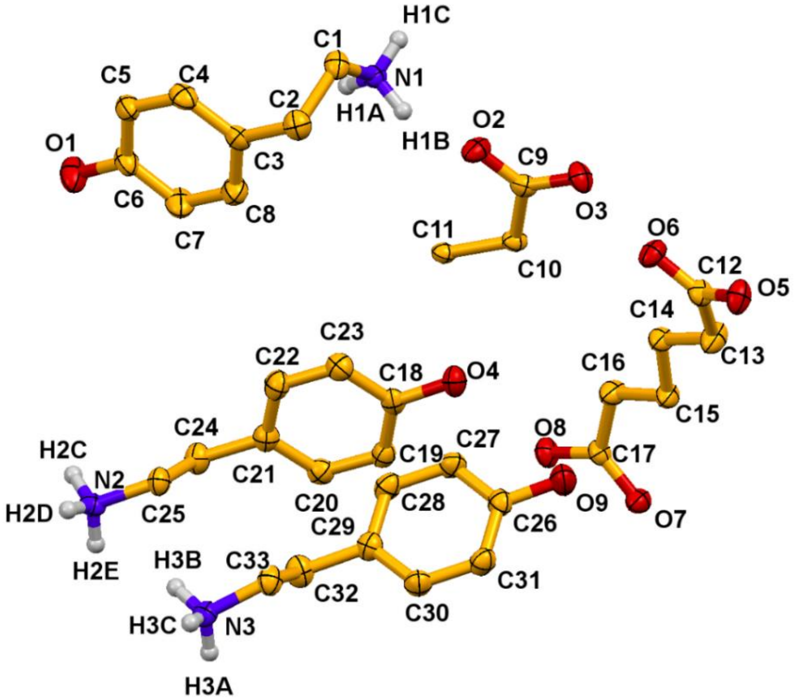

Fig. S4 ORTEP diagram of C_4•2TRM (50% probability).

Table S7 Hydrogen bonding table of C_4•2TRM.

D-H•••A	d(D-A)/Å	d(H•••A)/Å	d(D•••A)/Å	∠D-H•••A/°	Symmetry
O1-H1•••O3	0.84	1.82	2.656(2)	170	x, -1+y, z
N1-H1A•••O8	0.91	1.98	2.794(19)	148	1-x,-y,-z
N1-H1B•••O2	0.91	1.89	2.725(2)	151	x,y,z
N1-H1C•••O7	0.91	1.99	2.823(2)	152	-1+x,y,z
N1-H1C•••O8	0.91	2.48	3.189(2)	134	-1+x,y,z
N2-H2C•••O7	0.91	1.86	2.745(2)	162	x, -1+y, z
N2-H2D•••O5	0.91	1.87	2.768(2)	169	x,-1+y,z
N2-H2E•••O2	0.91	2.07	2.828(3)	139	1-x,-y,1-z
N2-H2E•••O3	0.91	2.30	3.159(3)	157	1+x,-1+y,z
N3-H3A•••O6	0.91	1.88	2.775(2)	169	1+x,-1+y,z
N3-H3B•••O6	0.91	1.93	2.797(3)	158	1-x,-y,1-z
N3-H3C•••O3	0.91	1.93	2.804(3)	161	x,y,z
O4-H4A•••O8	0.84	1.86	2.701(2)	179	1-x,1-y,1-z
O9-H9•••O5	0.84	1.83	2.663(3)	173	1-x,-1-y,-z

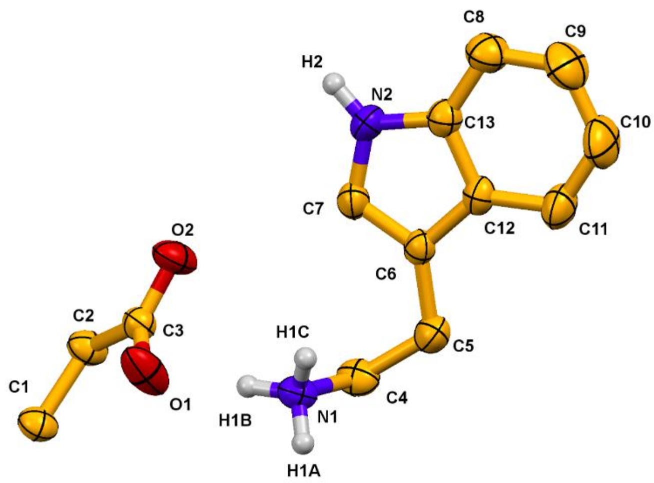

Fig. S5 ORTEP diagram of C_4•2TRP (50% probability).

Table S8 Hydrogen bonding table of C_4•2TRP.

D-H•••A	d(D-A)/Å	d(H•••A)/Å	d(D•••A)/Å	∠D-H•••A/°	Symmetry
N1-H1A•••O2	0.89	1.82	2.710(2)	174	x,-1+y,z
N2-H1B•••O1	0.89	1.86	2.745(2)	179	x,y,z
N1-H1C•••O1	0.89	2.59	3.366(3)	146	3/2-x,-1/2+y,1/2-z
N2-H1C•••O2	0.89	2.22	2.993(2)	145	3/2-x,1/2+y,1/2-z
N2-H2•••O1	0.93	2.03	2.763(2)	143	x,y,z

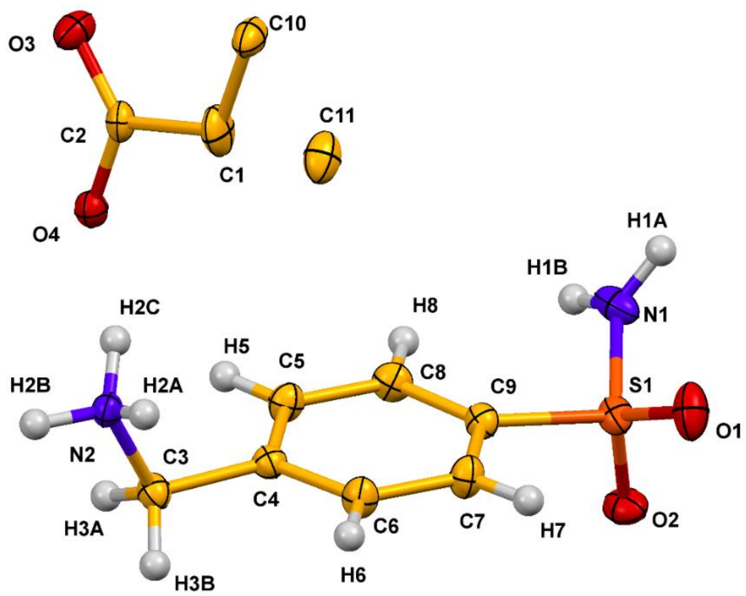

Fig. S6 ORTEP diagram of C_4•2MAF (50% probability).

Table S9 Hydrogen bonding table of C_4•2MAF.

D-H•••A	d(D-A)/Å	d(H•••A)/Å	d(D•••A)/Å	∠D-H•••A/°	Symmetry
N1-H1A•••O1	0.88	2.37	2.927(2)	122	3/2-x,-1/2+y,3/2-z
N2-H2A•••O3	0.91	1.87	3.176(2)	175	x,1+y,z
N1-H2B•••O4	0.91	1.91	2.757(2)	162	-x,1-y,1-z
N2-H2C•••O4	0.91	1.84	2.807(3)	164	x,y,z

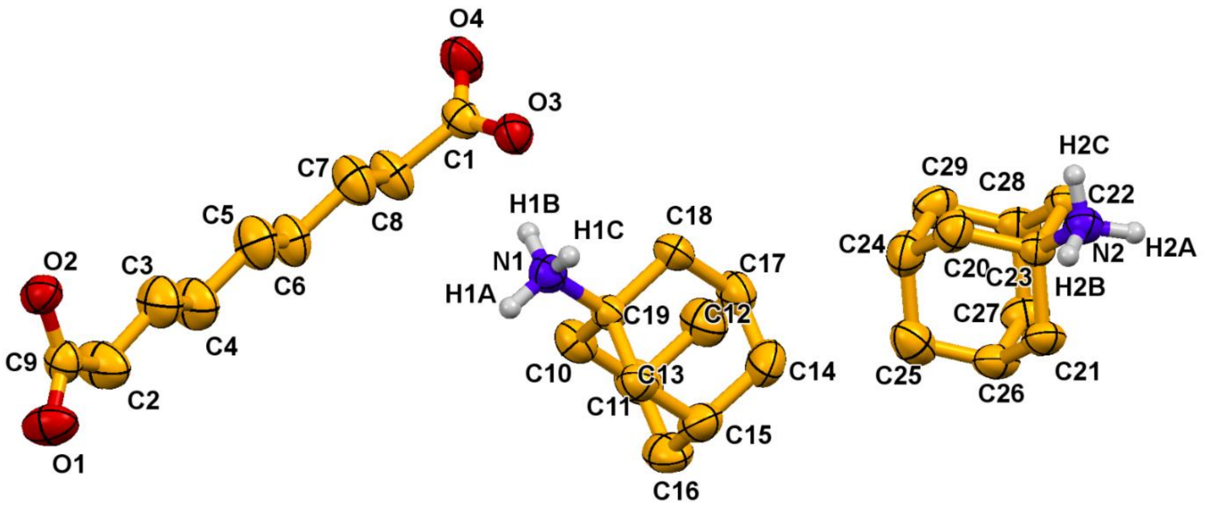

Fig. S7 ORTEP diagram of C_7•2AMN (50% probability).

Table S10 Hydrogen bonding table of C_7•2AMN.

D-H•••A	d(D-A)/Å	d(H•••A)/Å	d(D•••A)/Å	∠D-H•••A/°	Symmetry
N1-H1A•••O4	0.89	1.89	2.774(4)	173	x,-1+y,z
N1-H1B•••O3	0.89	1.92	2.792(4)	164	x,y,z
N1-H1C•••O3	0.89	2.04	2.930(4)	174	1-x,-1/2+y,3/2-z
N2-H2A•••O2	0.89	1.86	2.729(4)	167	1+x,1+y,z
N2-H2B•••O2	0.89	1.96	2.842(4)	169	1-x,1/2+y,3/2-z
N1-H2C•••O1	0.89	1.90	2.790(4)	174	1-x,3/2+y,3/2-z

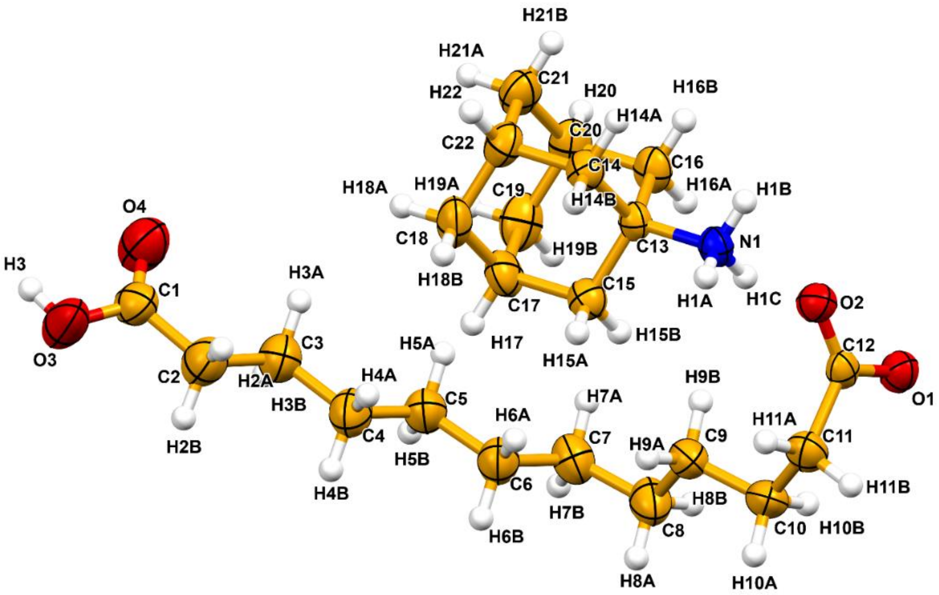

Fig. S8 ORTEP diagram of C10-H•AMN (50% probability).

Table S11 Hydrogen bonding table of C10-H•AMN.

D-H•••A	d(D-A)/Å	d(H•••A)/Å	d(D•••A)/Å	∠D-H•••A/°	Symmetry
N1-H1A•••O1	0.89	1.96	2.837(3)	169	-1+x, y, z
N1-H1B•••O2	0.89	2.01	2.871(3)	163	1-x, -y, 1-z
N1-H1C•••O2	0.89	1.92	2.776(3)	160	x, y, z
O3-H3•••O1	0.82	1.80	2.605(3)	168	-1+x, 1+y, z

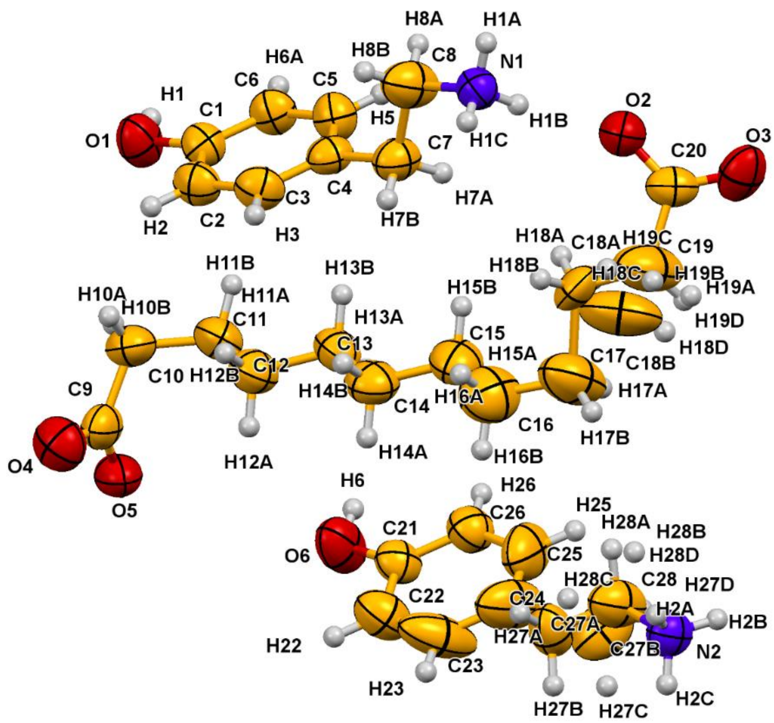

Fig. S9 ORTEP diagram of C_{10}•2TRM (50% probability).

Table S12 Hydrogen bonding table of C_{10}•2TRM.

D-H•••A	d(D-A)/Å	d(H•••A)/Å	d(D•••A)/Å	∠D-H•••A/°	Symmetry
O1-H1•••O3	0.82	1.91	2.712(8)	167	1/2+x,1-y,z
N1-H1A•••O5	0.89	1.95	2.817(9)	166	1-x,-y,-1/2+z
N1-H1B•••O2	0.89	1.97	2.834(9)	164	x,y,z
N1-H1C•••O3	0.89	1.87	2.765(8)	179	x,-1+y,z
N2-H1A•••O4	0.89	1.90	2.784(10)	174	-1/2+x,-y,z
N2-H2B•••O5	0.89	1.83	2.715(9)	177	-1/2+x,1-y,z
N2-H2C•••O2	0.89	1.93	2.823(9)	176	1/2-x,y,1/2+z
O6-H6•••O4	0.82	1.89	2.828(3)	166	x,1+y,z

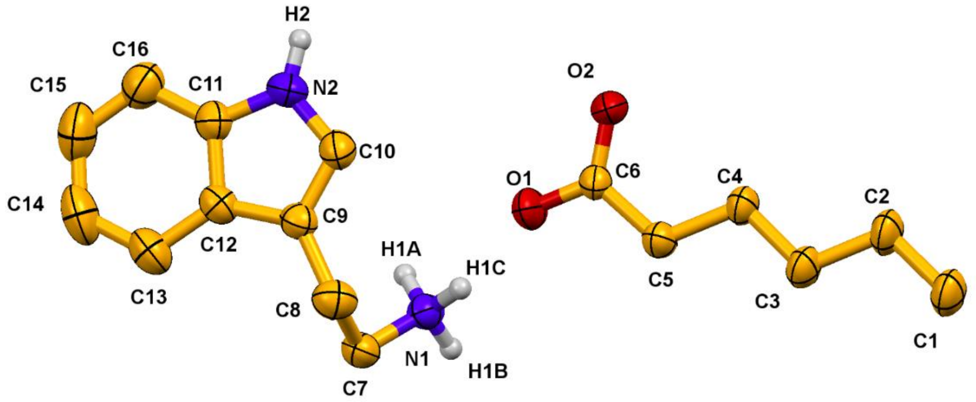

Fig. S10 ORTEP diagram of C_{10}•2TRP (50% probability).

Table S13 Hydrogen bonding table of C_{10}•2TRP.

D-H•••A	d(D-A)/Å	d(H•••A)/Å	d(D•••A)/Å	∠D-H•••A/°	Symmetry
N1-H1A•••O1	0.89	2.05	2.929(2)	168	1-x,2-y,1-z
N2-H1A•••O2	0.89	2.52	3.176(2)	131	1-x,2-y,1-z
N1-H1B•••O2	0.89	1.87	2.757(2)	177	1+x,y,z
N2-H1C•••O1	0.89	1.95	2.807(3)	161	x,y,z
N2-H2•••O2	0.86	2.14	2.848(3)	139	-x,2-y,1-z

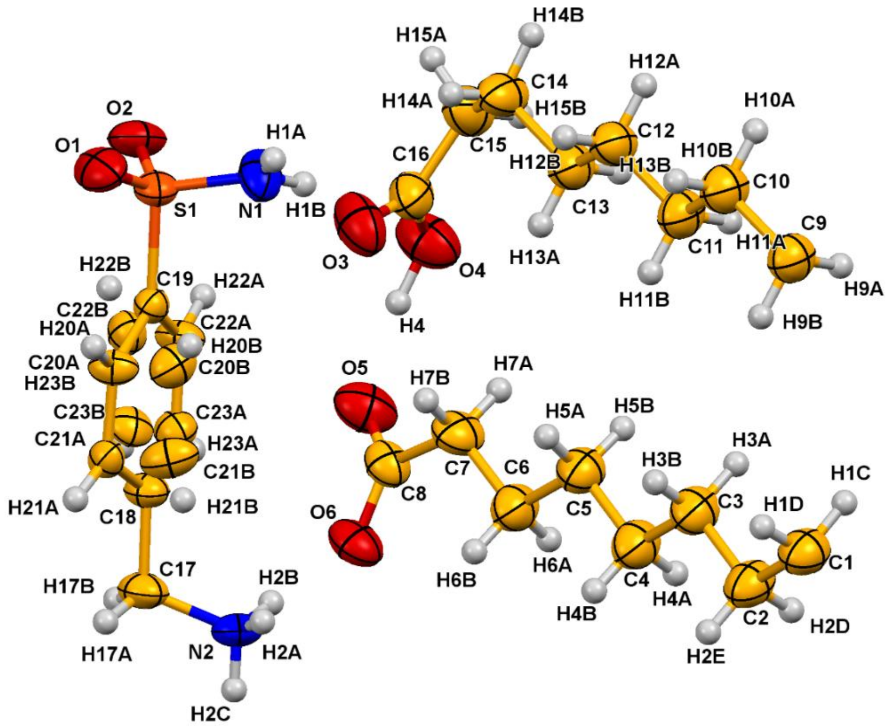

Fig. S11 ORTEP diagram of [C_{14}•2MAF].C_{14}-H_2 (50% probability).

Table S14 Hydrogen bonding table of [C_{14}•2MAF].C_{14}-H_2.

D-H•••A	d(D-A)/Å	d(H•••A)/Å	d(D•••A)/Å	∠D-H•••A/°	Symmetry
O1-H1•••O3	0.82	1.91	2.712(8)	167	1/2+x,1-y,z
N1-H1A•••O5	0.89	1.95	2.817(9)	166	1-x,-y,-1/2+z
N1-H1B•••O2	0.89	1.97	2.834(9)	164	x,y,z
N1-H1C•••O3	0.89	1.87	2.765(8)	179	x,-1+y,z
N2-H1A•••O4	0.89	1.90	2.784(10)	174	-1/2+x,-y,z
N2-H2B•••O5	0.89	1.83	2.715(9)	177	-1/2+x,1-y,z
N2-H2C•••O2	0.89	1.93	2.823(9)	176	1/2-x,y,1/2+z
O6-H6•••O4	0.82	1.89	2.828(3)	166	x,1+y,z

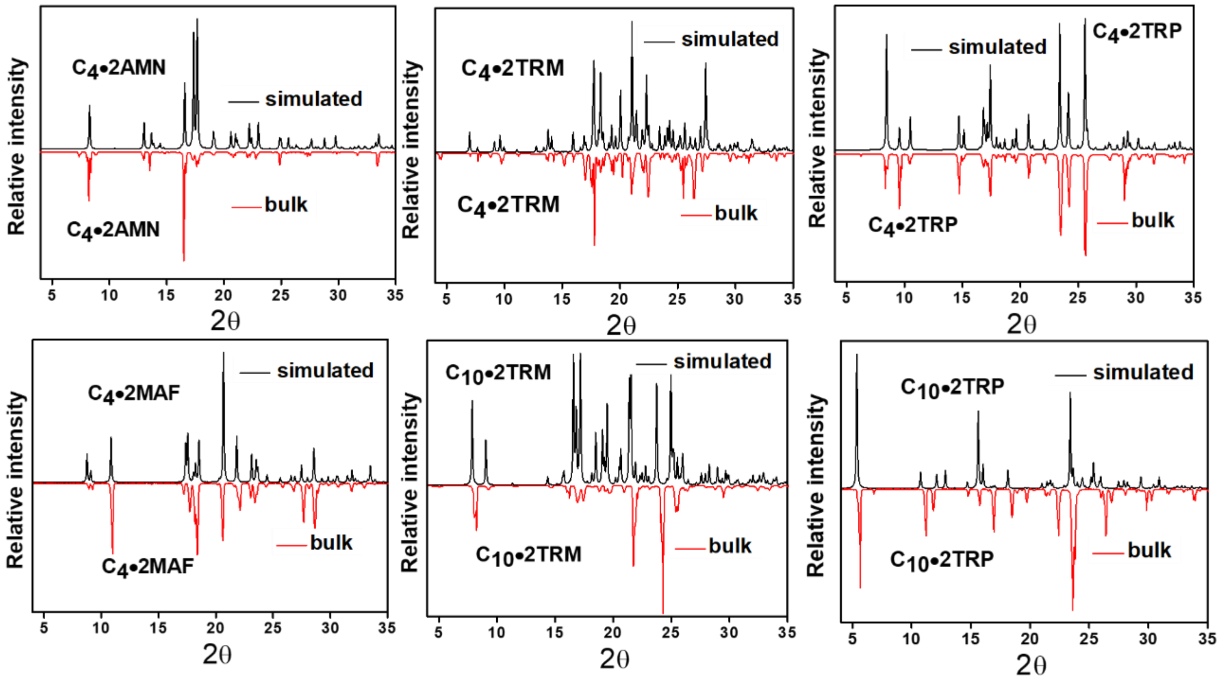

Fig. S12 PXRD (Simulated vs Bulk) comparison plots of various salts.

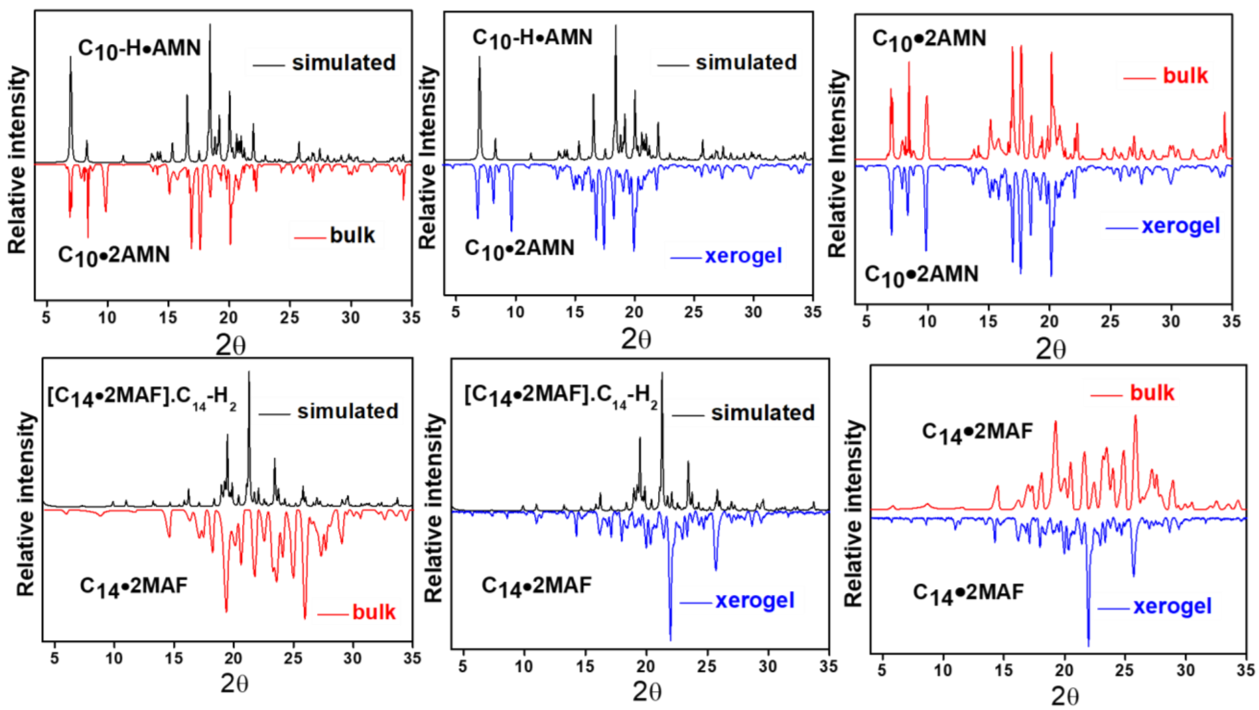

Fig. S13 PXRD plots of C_{10}•2AMN and C_{14}•2MAF.

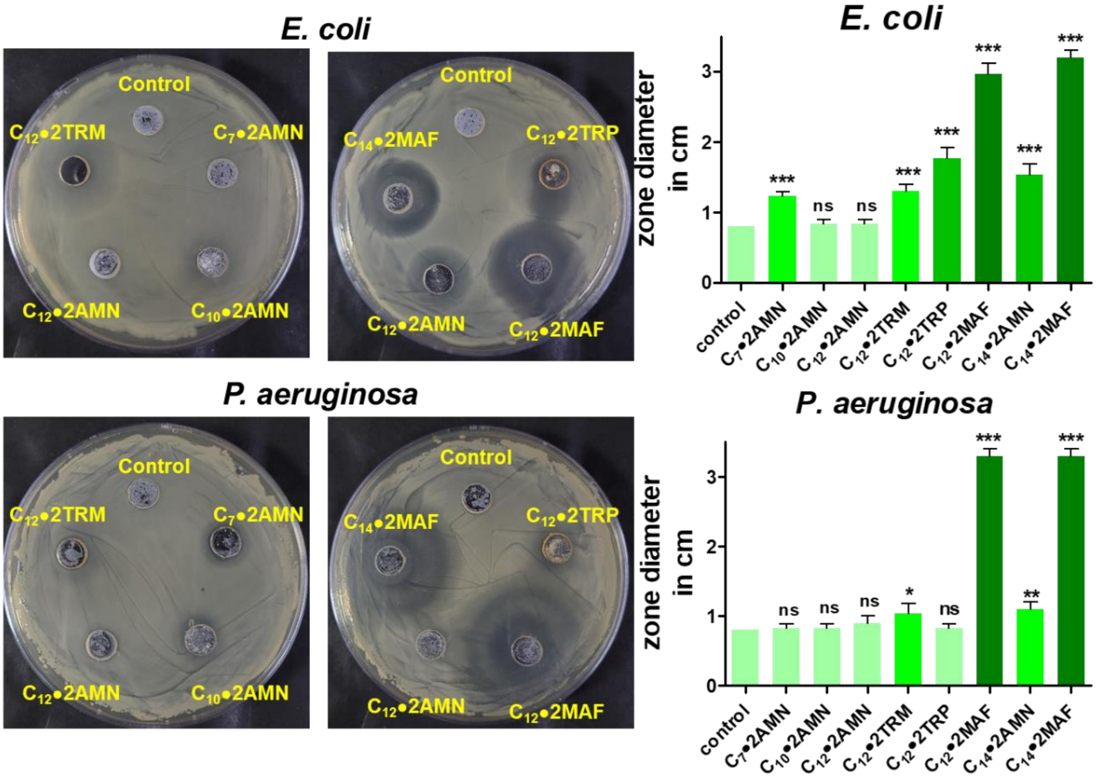

Fig. S14 Zone Inhibition Assay of the gelators against Gram-negative bacterial *E. coli* and *P. aeruginosa* In graphs, data were represented as mean+SD (n=3); where *p<0.05, **p<0.01, ***p<0.001 and ns is non-significant.

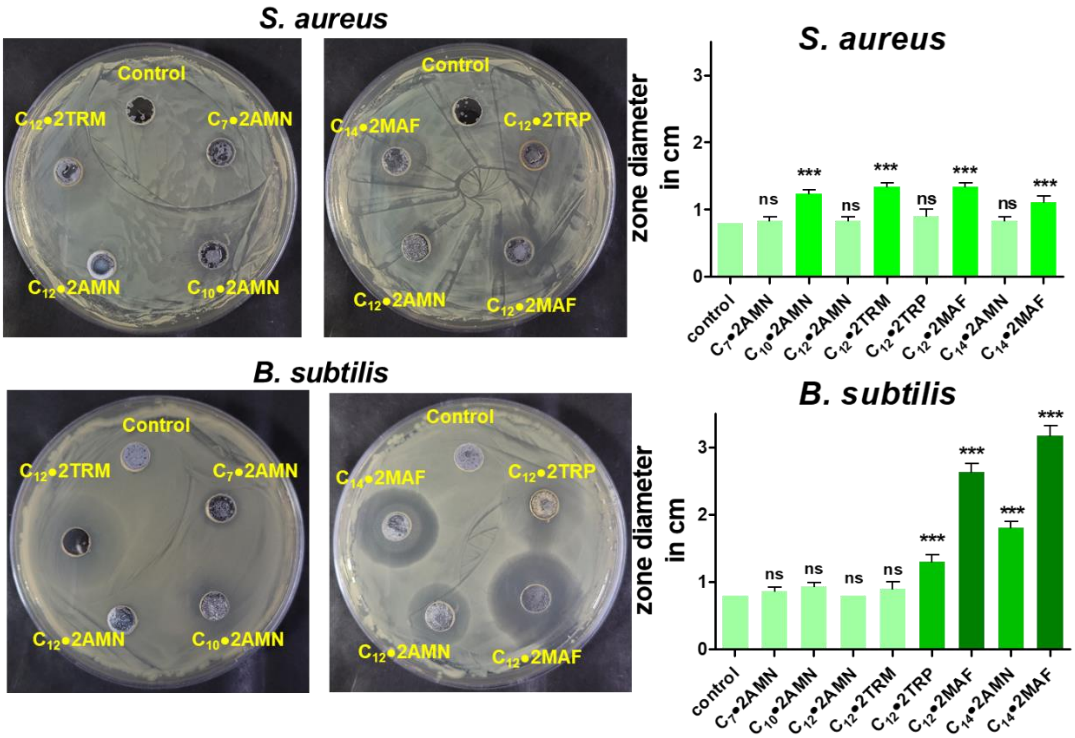

Fig. S15 Zone Inhibition Assay of the gelators against Gram-positive bacterial S. aureus and B. subtilis In graphs, data were represented as mean+SD (n=3); where *p<0.05, **p<0.01, ***p<0.001 and ns is non-significa

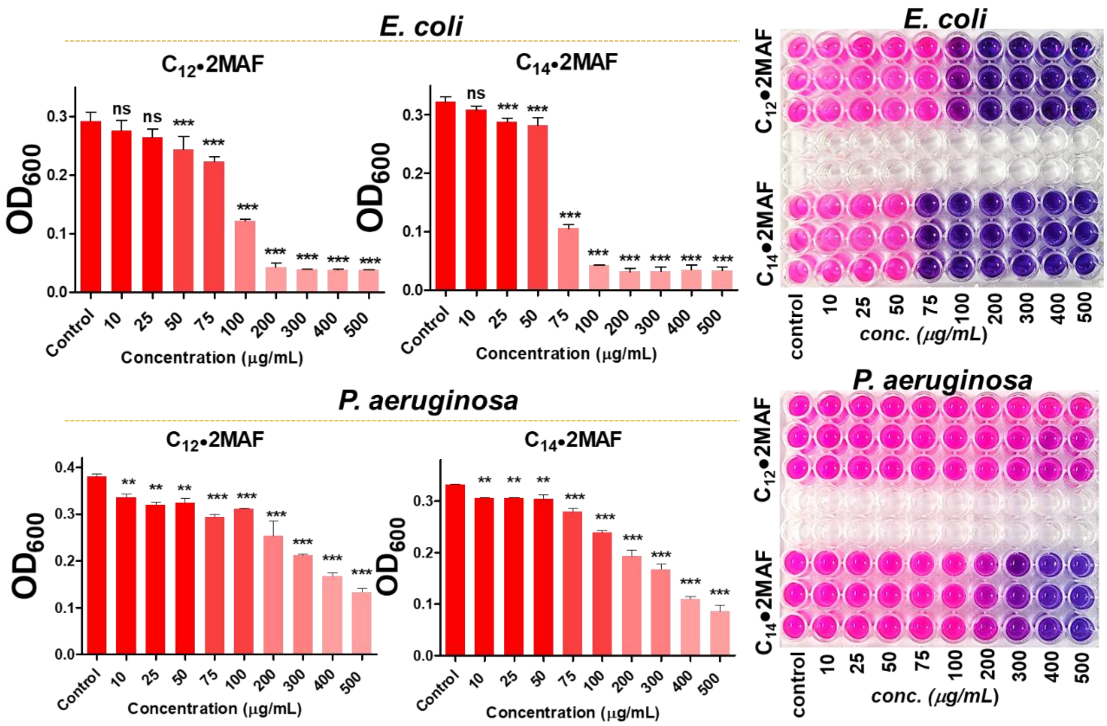

Fig. S16 Determination of MIC (Turbidity and Resazurin assay) of C_{12}•2MAF and C_{14}•2MAF against Gram-negative bacterial E. coli and P. aeruginosa. In graphs, data were represented as mean+SD (n=3); where *p<0.05, **p<0.01, ***p<0.001 and ns is non-significant.

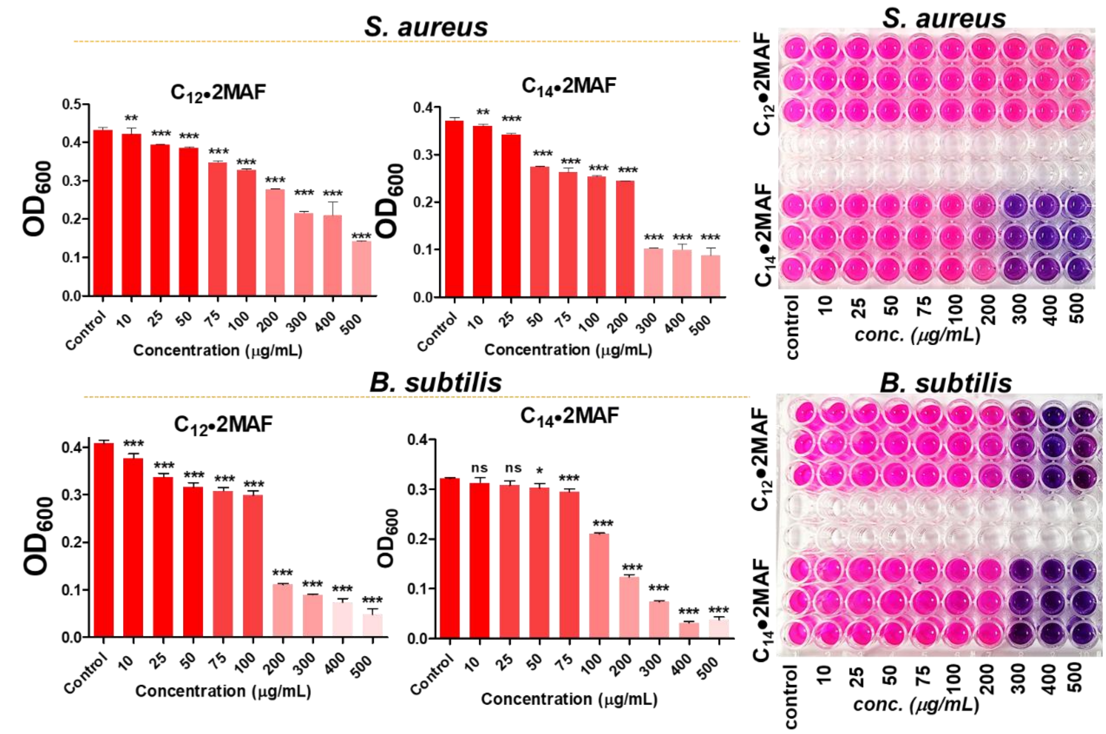

Fig. S17 Determination of MIC (Turbidity and Resazurin assay) of C_{12}•2MAF and C_{14}•2MAF against Gram-positive bacterial S. aureus and B. subtilis. In graphs, data were represented as mean+SD (n=3); where *p<0.05, **p<0.01, ***p<0.001 and ns is non-significant.

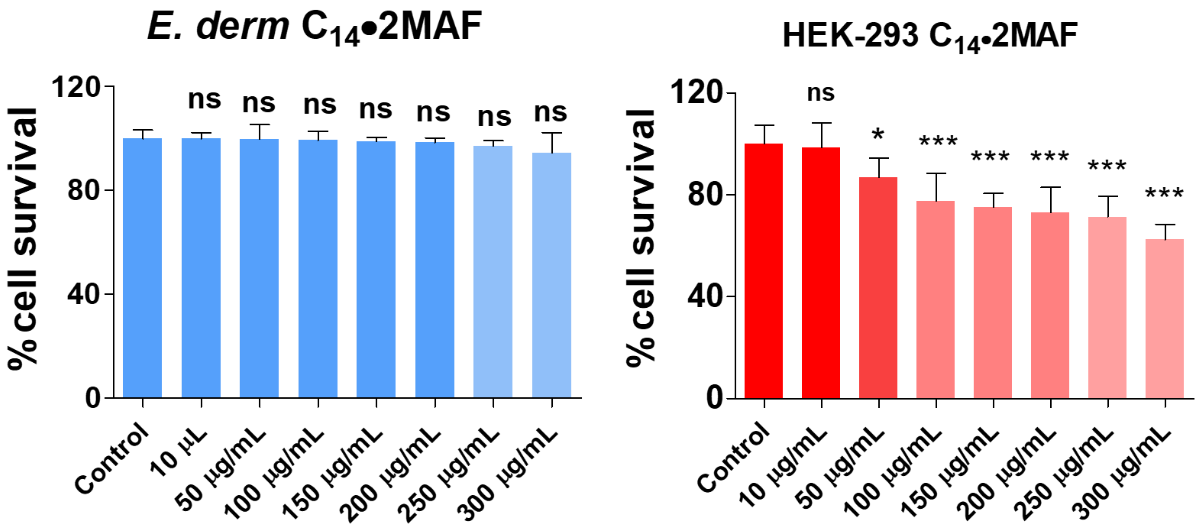

Fig. S18 MTT assay of C_{14}•2MAF against E. derm and HEK-293 cell lines. In graphs, data were represented as mean+SD (n=3); where *p<0.05, **p<0.01, ***p<0.001 and ns is non-significant.

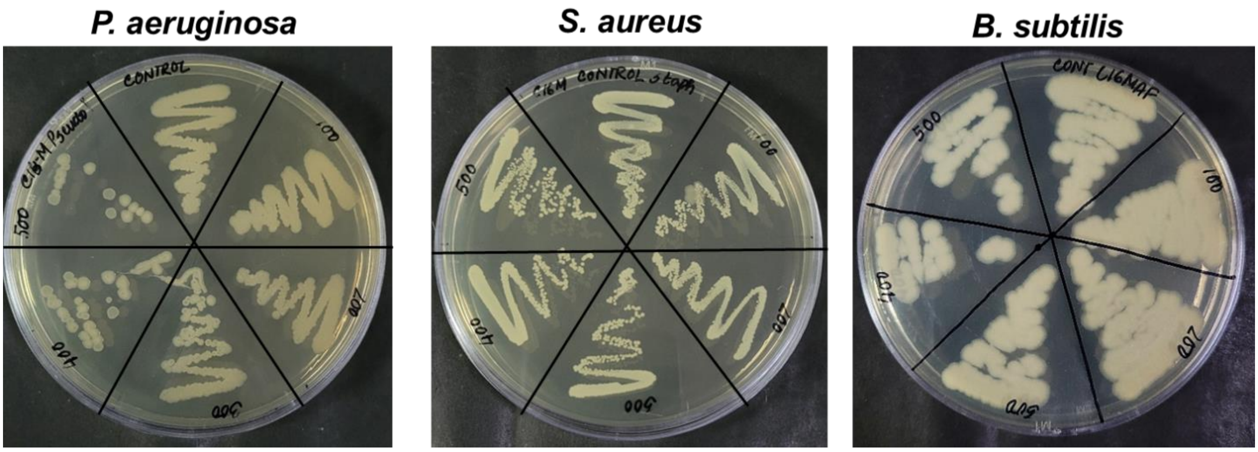

Fig. S19 Dose dependent bacterial colony inhibition assay of C_{14}•2MAF against P. aeruginosa, S. aureus and B. subtilis.

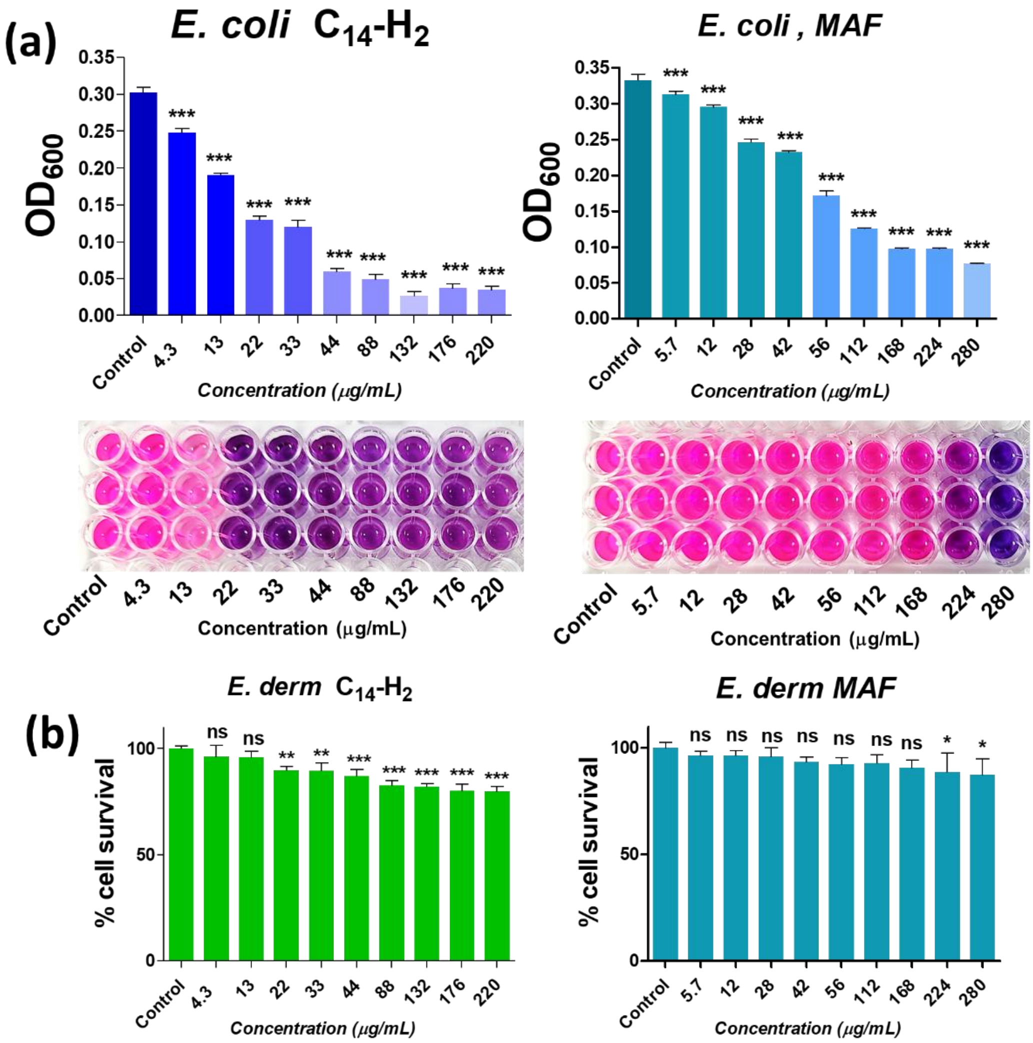

Fig. S20 (a) Turbidity and Resazurin assay of the components present in gelator salt C_{14}•2MAF (1 equivalent of C_{14}-H_2 and 2 equivalents of MAF present in the corresponding weights) against *E. coli.* (b) MTT assay of components C_{14}-H_2 and MAF against *E. derm*. In graphs, data were represented as mean+SD (n=3); where $^*p<0.05$, $^{**}p<0.01$, $^{***}p<0.001$ and ns is non-significant.

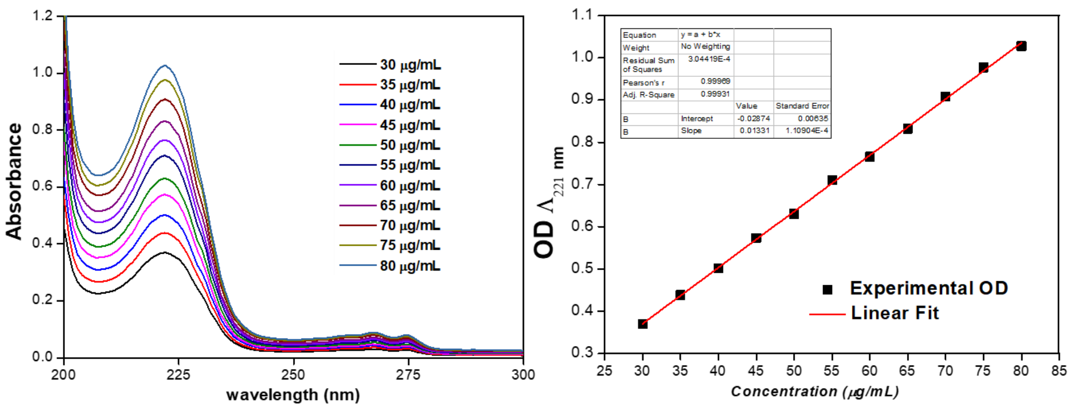

Fig. S21 Standard calibration curves of C_{14}•2MAF in water.

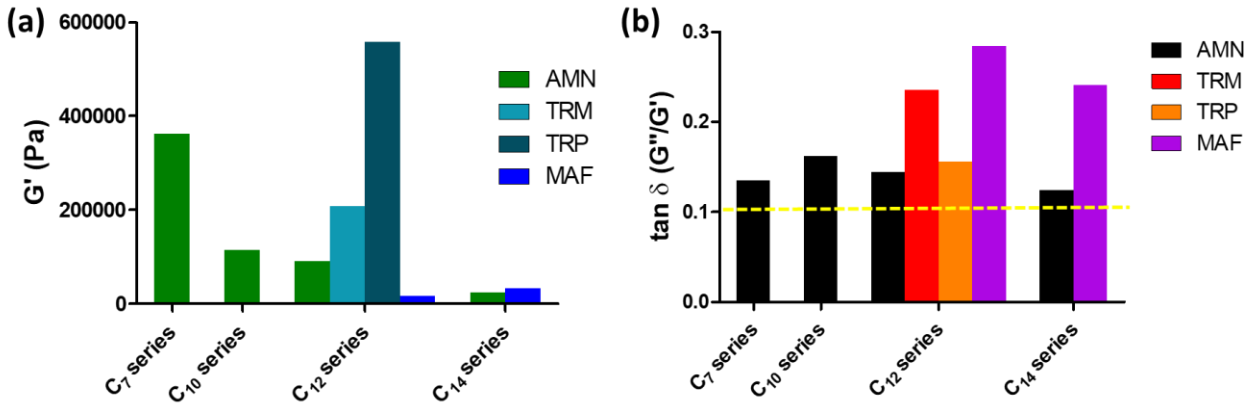

Fig. 22 (a) G' values of all MS gels (b) tan δ (G''/G') of the MS gels reported in this project.

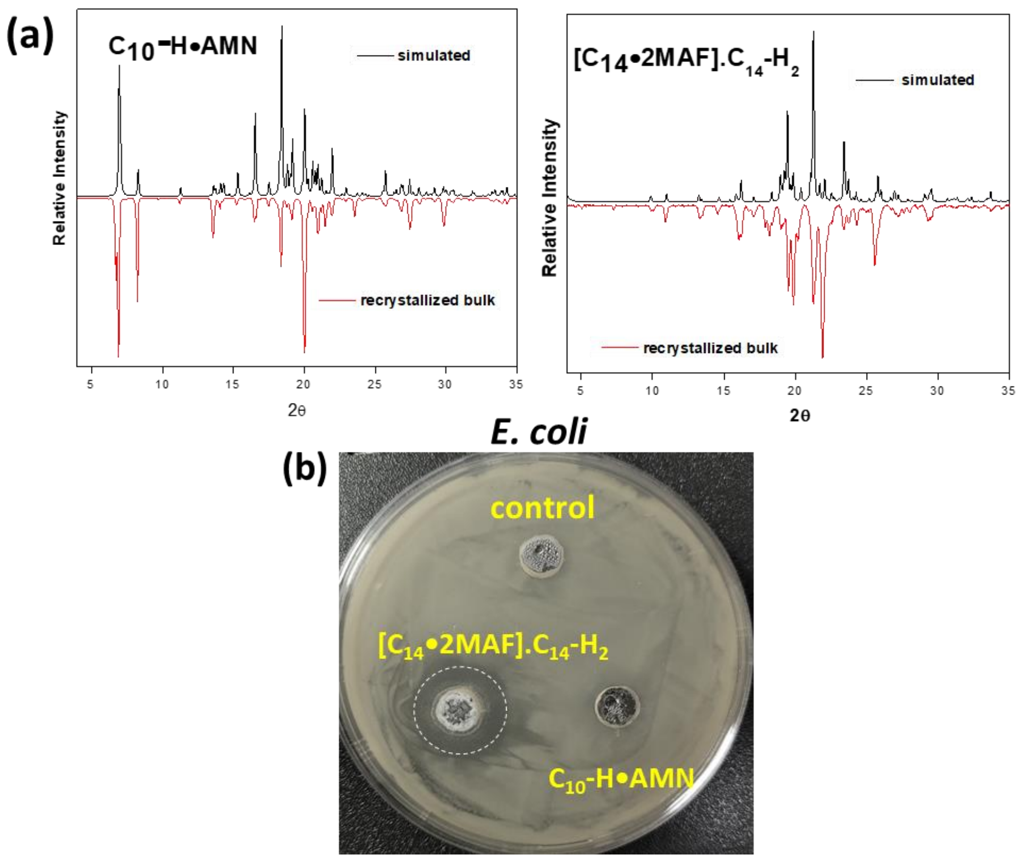

Fig. 23 (a) PXRD plots (Simulated vs Recrystallized bulks) of C_{10}-H•AMN and [C_{14}•2MAF].C_{14}-H_2 (b) Anti-bacterial zone inhibition assay of C_{10}-H•AMN and [C_{14}•2MAF].C_{14}-H_2 against *E. coli.*